

Reconstructing the spatial structure of quantum correlations in materials

Allen Scheie^{1,*}, Pontus Laurell², Elbio Dagotto^{2,3}, D. Alan Tennant², and Tommaso Roscilde^{4,†}

¹*MPA-Q, Los Alamos National Laboratory, Los Alamos, New Mexico 87545, USA*

²*Department of Physics and Astronomy, University of Tennessee, Knoxville, Tennessee 37996, USA*

³*Materials Science and Technology Division, Oak Ridge National Laboratory, Oak Ridge, Tennessee 37831, USA*

⁴*Université Lyon, ENS de Lyon, CNRS, Laboratoire de Physique, F-69342 Lyon, France*



(Received 15 September 2023; revised 11 April 2024; accepted 11 June 2024; published 19 August 2024)

Quantum correlations are a fundamental property of quantum many-body states. Yet they remain experimentally elusive, hindering certification of genuine quantum behavior, especially in quantum materials. Here we show that the momentum-dependent dynamical susceptibility measured via inelastic neutron scattering enables the systematic reconstruction of a general family of quantum correlation functions, which express the degree of quantum coherence in the fluctuations of two spins at an arbitrary mutual distance. Using neutron scattering data for the compound KCuF_3 —a system of weakly coupled $S = 1/2$ Heisenberg chains—and numerically exact quantum Monte Carlo data, we show that quantum correlations possess a radically different spatial structure with respect to conventional correlations. Indeed, they exhibit a different emergent length scale—the quantum coherence length—which is finite at any finite temperature (including when long-range magnetic order develops). Moreover, we show theoretically that coupled Heisenberg spin chains exhibit a form of quantum monogamy, with a trade-off between quantum correlations along and transverse to the spin chains. These results highlight real-space quantum correlators as an informative, model-independent means of probing the underlying quantum state of real quantum materials.

DOI: [10.1103/PhysRevResearch.6.033183](https://doi.org/10.1103/PhysRevResearch.6.033183)

I. INTRODUCTION

Quantum superpositions are among the most profound and fascinating phenomena in nature. They lead to a variety of quantum correlations, including entanglement [1] and Bell nonlocality [2], both considered resources in quantum information processing. Such quantum correlations have been experimentally demonstrated in systems isolated from their environment with few degrees of freedom, such as photons [3,4], atoms [5–7], and superconducting circuits [8,9]. However, quantum materials, which host a wealth of exotic physical states [10], sit at the opposite end of the many-body spectrum. Their quantum-mechanical degrees of freedom are of order Avogadro’s number and interact strongly and locally, so their physics is very sensitive to the underlying system geometry. These interacting degrees of freedom produce some very exotic phenomena, which is why quantum materials are so intensely studied [10,11]. However, despite receiving much attention, the underlying quantum states of quantum materials are often unknown. Certifying the quantum superposition nature of such systems and understanding the effects of

geometry and dimensionality of interactions on quantum correlations represent grand challenges for quantum condensed matter physics, as well as new opportunities to understand the role of quantum mechanics in macroscopic systems.

Fortunately, quantum information theory offers powerful tools for probing quantum superpositions in generic systems in the form of coherence measures [12–15]. Here we focus on observable-based measures, which probe the coherences of a quantum state when represented in the eigenbasis of an observable, i.e., the noncommutativity between the observable and the density matrix. Typically, coherences are studied via interferometric experiments [14] and provide the basis of the metrological sensitivity of a quantum state. Unfortunately, interferometry is rarely accessible in the solid-state context, and the density matrix itself is not accessible either. However, recent works [16–18] related quantum coherence measures for quantum states in thermal equilibrium to linear response functions, which are directly accessible to spectroscopic techniques such as light scattering, AC magnetometry, and inelastic neutron scattering. This link allowed neutron scattering experiments on quantum magnets [19–21] to reconstruct their quantum Fisher information (QFI) [14,22]. Measurements of QFI associated with order parameters have, in turn, led to estimates of the entanglement depth, i.e., a lower bound on the minimal number of entangled degrees of freedom in a multipartite entangled state, in the low-temperature phase of low-dimensional magnets, such as spin chains and triangular antiferromagnets [20,21,23].

In this work we show that a Fourier analysis of the linear response function measured in neutron scattering, reweighted

*Contact author: scheie@lanl.gov

†Contact author: tommaso.roskilde@ens-lyon.fr

Published by the American Physical Society under the terms of the [Creative Commons Attribution 4.0 International](https://creativecommons.org/licenses/by/4.0/) license. Further distribution of this work must maintain attribution to the author(s) and the published article’s title, journal citation, and DOI.

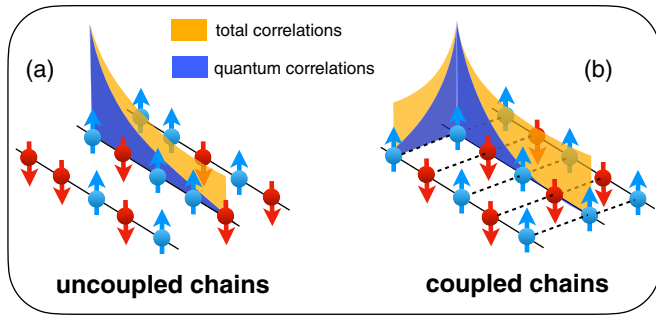


FIG. 1. Total vs quantum correlations in $S = 1/2$ Heisenberg chains. (a) Uncoupled 1D chains and (b) chains subject to interchain coupling. Total and quantum correlations are widely different at any finite temperature. Whereas total correlations are enhanced in all directions when the chains are coupled at fixed temperature, quantum correlations are redistributed spatially (at low temperatures) due to an effective form of monogamy (i.e., mutual exclusion). This illustration depicts a two-dimensional system for clarity, but in the text we consider a three-dimensional system with chains coupled along both directions perpendicular to the chains.

by an appropriate quantum filter function, allows one to extract the full spatial structure of quantum correlations in a model-free manner (i.e., it is applicable to arbitrarily complex systems beyond the reach of simulation techniques). Importantly, as we show in this study, such analysis can reveal surprising and new information, even for very well studied models and materials.

Making use of neutron scattering data on the $S = 1/2$ Heisenberg antiferromagnetic chain system KCuF_3 [20,24,25] and quantum Monte Carlo (QMC) simulations, we show that these quantum correlation functions share a common spatial structure, and unlike the ordinary correlation function, they exhibit an exponential decay at all finite temperatures, with an emergent quantum coherence length [26] which differs substantially from the ordinary correlation length. We provide, therefore, a clear experimental observation of the short-range nature of quantum correlations at finite temperature, in agreement with recent numerical and analytical results [18,26,27]. We also show numerically that weakly coupled antiferromagnetic chains at low temperature exhibit stronger quantum correlations at short range than strongly coupled chains due to an effective form of “monogamy” (i.e., mutual exclusion) of quantum correlations; see Fig. 1 for a sketch summarizing the main results.

II. THEORY OF QUANTUM CORRELATION FUNCTIONS

Quantum correlation functions can generally be defined as the difference between two types of correlations that are classically equivalent and that coincide quantum mechanically only when the correlated observables commute with the state, e.g., the statistical correlations of two fluctuating observables, and the response of an observable to a field coupling to the other observable. This latter notion coincides with the *quantum covariance* introduced in Ref. [26], but related quantities (connected to QFI or the Wigner-Yanase-Dyson skew information (SI) [28]) can also be defined.

For a lattice quantum system, we consider local Hermitian bounded operators O_i , with i being the lattice site index, and introduce their sum, building up the extensive observable $O = \sum_i O_i$. We then consider the two-site dynamical susceptibility $\chi''_{O_i, O_j}(\omega)$ [29], expressing the out-of-phase variation of the expectation value of O_i in response to a periodic field oscillating at frequency ω and coupling to O_j . Its mathematical expression reads $\chi''_{O_i, O_j}(\omega) = -\int dt/\hbar e^{-i\omega t} \langle [O_i(t), O_j(0)] \rangle$, where $\langle \dots \rangle = \text{Tr}[(\dots)\rho]$ represents the thermal equilibrium average at temperature T when $\rho = e^{-\beta H}/\mathcal{Z}$, with $\beta = (k_B T)^{-1}$, H being the system Hamiltonian, and \mathcal{Z} being the partition function. A family of quantum correlation functions can then be related to the two-site dynamical susceptibility via an integration over frequency, weighted by an appropriate quantum filter function $h(\beta\hbar\omega)$,

$$C[O_i, O_j; h, \rho] = \frac{1}{\pi} \int_0^\infty d(\hbar\omega) h(\beta\hbar\omega) \chi''_{O_i, O_j}(\omega). \quad (1)$$

For C to be a well-defined measure of quantum coherence, the function $h(x)$ must satisfy basic mathematical properties [30–33], namely, $h(x) \sim x$ when $x \rightarrow 0$ and $h(x \rightarrow \infty) = 1$; in this way it acts as a high-pass filter for frequencies $\hbar\omega \gg k_B T$, associated with excitation modes behaving quantum mechanically at temperature T . Summing Eq. (1) over the spatial indices yields a quantum coherence measure associated with the observable O , $I[O; h, \rho] = \sum_{ij} C[O_i, O_j; h, \rho]$. Notable special cases include (1) the QFI, $I[O; 4h_{\text{QFI}}, \rho] = \text{QFI}(O; \rho)$, for which [16,32,33]

$$h_{\text{QFI}}(x) = \tanh(x/2), \quad (2)$$

where

$$\begin{aligned} \text{QFIM}[O_i, O_j; \rho] &= C[O_i, O_j; 4h_{\text{QFI}}, \rho] \\ &= \frac{1}{\pi} \int_0^\infty d(\hbar\omega) 4h_{\text{QFI}}(\beta\hbar\omega) \chi''_{O_i, O_j}(\omega) \end{aligned} \quad (3)$$

expresses the quantum Fisher information matrix (QFIM) [34]; (2) the quantum variance Var_Q [17], $I[O; h_{\text{Var}_Q}, \rho] = \text{Var}_Q(O; \rho)$, for which

$$h_{\text{Var}_Q}(x) = \mathcal{L}(x/2), \quad (4)$$

where $\mathcal{L}(x) = \coth x - 1/x$ is the Langevin function and

$$\begin{aligned} \text{Cov}_Q[O_i, O_j; \rho] &= C[O_i, O_j; h_{\text{Var}_Q}, \rho] \\ &= \frac{1}{\pi} \int_0^\infty d(\hbar\omega) h_{\text{Var}_Q}(\beta\hbar\omega) \chi''_{O_i, O_j}(\omega) \end{aligned} \quad (5)$$

expresses the quantum covariance Cov_Q [18,26]; and (3) the Wigner-Yanase-Dyson SI [28], $I[O; h_\alpha, \rho] = \text{SI}_\alpha(O; \rho)$, for which

$$h_\alpha(x) = \frac{\cosh(x/2) - \cosh[(\alpha - 1/2)x]}{\sinh(x/2)}, \quad (6)$$

where $0 < \alpha < 1$ is a parameter that takes the value of $\alpha = 1/2$ in the original Wigner-Yanase definition [28], with

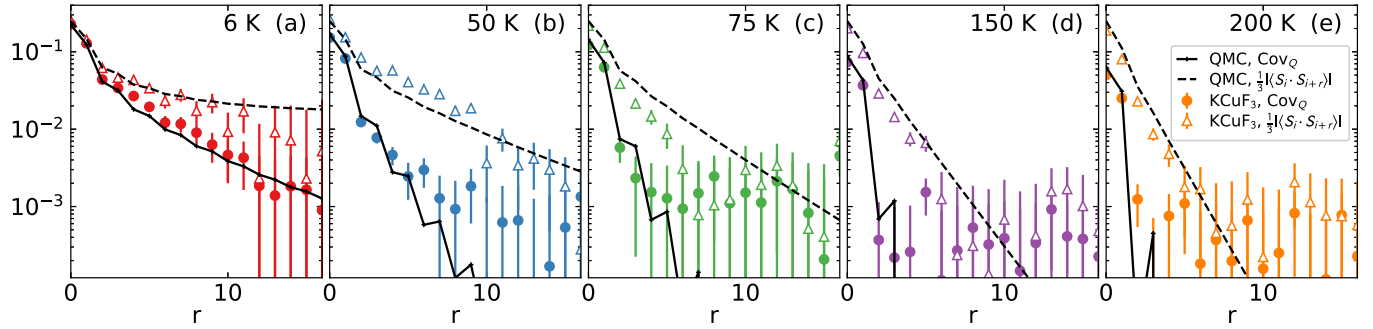


FIG. 2. Total vs quantum correlations in KCuF_3 . Reconstructed total and quantum correlations [expressed by the quantum covariance Cov_Q , Eq. (5)] along the spin chains of KCuF_3 at various temperatures, compared with numerically exact QMC data. The error bars represent one standard deviation uncertainty.

$h_{1/2} = \tanh(x/4)$, and

$$\begin{aligned} \text{SIM}_\alpha[O_i, O_j; \rho] &= C[O_i, O_j; h_\alpha, \rho] \\ &= \frac{1}{\pi} \int_0^\infty d(\hbar\omega) h_\alpha(\beta\hbar\omega) \chi''_{O_i, O_j}(\omega) \end{aligned} \quad (7)$$

expresses the skew information matrix (SIM). Var_Q and Cov_Q can, in fact, be obtained as the average of SI_α and SIM_α , respectively, on the α index since $\int_0^1 d\alpha h_\alpha(x) = \mathcal{L}(x/2)$. All of the above quantities are intimately linked by the inequality chain (for $\alpha = 1/2$) $\text{Var}_Q[O; \rho] \leq \text{SI}_{1/2}[O; \rho] \leq \text{QFI}[O; \rho]/4 \leq 2\text{SI}_{1/2}[O; \rho] \leq 3\text{Var}_Q[O; \rho]$.

In this work we focus mainly on the quantum covariance Cov_Q [18,26]. This definition corresponds to the difference between static correlations and static response functions [17,26], and consequently, quantum variance and covariance can be calculated efficiently with QMC. (The QFI and QFIM, meanwhile, require instead full reconstruction of the dynamical susceptibility, which is not accessible to QMC directly due to a notoriously ill-defined analytical continuation of time-dependent correlations from imaginary to real time [35].)

III. QUANTUM CORRELATION FUNCTIONS FROM NEUTRON SCATTERING

Inelastic neutron scattering measures the dynamical structure factor $S(\mathbf{Q}, \omega)$ related to the momentum-dependent dynamical susceptibility via the fluctuation-dissipation theorem $\chi''_{\mu\nu}(\mathbf{Q}, \omega) = \pi(1 - e^{-\hbar\omega\beta})S_{\mu\nu}(\mathbf{Q}, \omega)$ [36], where $\chi''_{\mu\nu}(\mathbf{Q}, \omega) = -\int dt/\hbar e^{-i\omega t} \langle [S_{\mathbf{Q}}^\mu(t), S_{-\mathbf{Q}}^\nu(0)] \rangle$, with $\mu, \nu = x, y, z$, and $S_{\mathbf{Q}}^\mu = N^{-1/2} \sum_i e^{i\mathbf{Q}\cdot\mathbf{r}_i} S_i^\mu$ is the Fourier transform of the S_i^μ operators for a lattice with N sites. If $S(\mathbf{Q}, \omega)$ is measured across the full Brillouin zone, its inverse Fourier transform allows one to reconstruct the two-site dynamical susceptibility and calculate the quantum correlation functions.

To test this idea, we use the neutron scattering data reported in Ref. [37] for KCuF_3 ; see Appendix A for details. This material is an ideal approximation of a system of coupled Heisenberg $S = 1/2$ chains [25,38],

$$H = J \sum_{\langle ij \rangle: \text{chains}} \mathbf{S}_i \cdot \mathbf{S}_j + J_\perp \sum_{\langle lm \rangle: \text{inter}} \mathbf{S}_l \cdot \mathbf{S}_m, \quad (8)$$

where \mathbf{S}_i is a $S = 1/2$ spin operator at site i ; the first sum runs on nearest-neighbor bonds along the chains, and the second runs on bonds connecting nearest-neighbor chains to form a tetragonal lattice. KCuF_3 has weak interchain coupling $J_\perp = -1.6$ meV compared to the in-chain coupling $J = 34$ meV [39], causing weak long-range Néel order to appear at a low critical temperature $T_N = 39$ K $\approx 0.1J$. Nevertheless, many salient features of the one-dimensional physics (such as fractional excitations at sufficiently high energy [25]) are preserved to low T in spite of the long-range ordering.

In magnetic scattering such as that from KCuF_3 the measured dynamical susceptibility is $\tilde{\chi}''(\mathbf{Q}, \omega) = \sum_{\mu, \nu=x,y,z} (\delta_{\mu\nu} - \hat{Q}_\mu \hat{Q}_\nu) \chi''_{\mu\nu}(\mathbf{Q}, \omega)$ [40], where \hat{Q}_μ are the $\mu = x, y, z$ components of the normalized scattering vector. In the Heisenberg (isotropic) limit, the spin components act identically, and $\tilde{\chi}''(\mathbf{Q}, \omega) = \frac{2}{3} \sum_{\mu=x,y,z} \chi''_{\mu\mu}(\mathbf{Q}, \omega)$. The two-site spin susceptibility along $\hat{\mu}$, $\chi''_{S_i^\mu S_j^\mu}(\omega)$, is obtained with the spatial Fourier transform of $\chi''_{\mu\mu}(\mathbf{Q}, \omega)$. We also define the two-site dynamical susceptibility $\chi''_{ij}(\omega) = \frac{1}{3} \sum_{\mu=x,y,z} \chi''_{S_i^\mu S_j^\mu}(\omega)$, including the prefactor $1/3$ for convenience. Thus, the quantum correlation functions defined above can then be reconstructed, along with the total correlation function

$$C_{\text{tot}}(i, j) = \frac{1}{3} \langle \mathbf{S}_i \cdot \mathbf{S}_j \rangle = \frac{1}{\pi} \int d(\hbar\omega) \coth(\beta\hbar\omega/2) \chi''_{ij}(\omega), \quad (9)$$

where the coth factor converts dynamic susceptibility back to $S(\mathbf{Q}, \omega)$ via the fluctuation dissipation theorem [36]. The total correlations are expected to exhibit an exponentially decaying behavior for $T > T_N$, $C_{\text{tot}}(i, j) \sim \exp(-|i-j|/\xi)$, with ξ being the correlation length, while the divergence of ξ at T_N entails the appearance of long-range correlations. On the other hand, the quantum covariance Cov_Q is expected to exhibit an exponential decay at any finite temperature, $\text{Cov}_Q(i, j) \sim \exp(-|i-j|/\xi_Q)$, with ξ_Q defining the quantum coherence length, which is finite at any finite temperature and coincides with ξ only for $T \rightarrow 0$. This behavior for Cov_Q was numerically observed via QMC in Refs. [18,26] and was established as a rigorous result only recently [27]. Yet an experimental measurement of ξ_Q is still lacking to date.

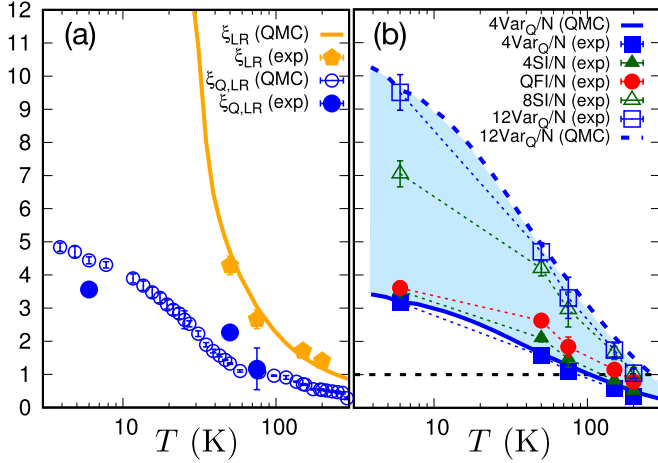


FIG. 3. Quantum coherence length vs entanglement depth. (a) Quantum coherence length ξ_Q vs total correlation length ξ as a function of temperature. (b) Entanglement depth estimated via the quantum fluctuations of the in-chain staggered magnetization, namely, $4\text{Var}_Q(M_{s,\text{chain}})/N$ and $\text{QFI}(M_{s,\text{chain}})/N$. The plot also shows $12\text{Var}_Q/N$, which is an upper bound on $\text{QFI}(M_{s,\text{chain}})/N$, as well as the lower and upper bounds on $\text{QFI}(M_{s,\text{chain}})/N$ from the skew information, $4\text{SI}/N$ and $8\text{SI}/N$. Both panels compare QMC data and experimental data for KCuF_3 . The error bars represent one standard deviation uncertainty.

IV. QUANTUM CORRELATIONS FOR KCuF_3

Figure 2 compares $C_{\text{tot}}(i, j)$ and Cov_Q for sites i and j belonging to the same chain, as reconstructed from the neutron scattering structure factor of KCuF_3 at various temperatures ($T = 6, 50, 75, 150,$ and 200 K) above and below T_N . The experimental data are compared with QMC data (obtained via the stochastic series expansion method [41]) for a 10×10 array of 100-site spin chains. The experimental results beautifully match the theoretical ones, including a detailed structure clearly visible at short ranges. The vast difference between the total correlation length and the emergent quantum coherence length is apparent: while the total correlations go from exponentially decaying (above T_N) to decaying to a finite value (below T_N), the quantum covariance clearly remains short range at all temperatures, with a decay length ξ_Q significantly smaller than ξ . This implies that quantum correlations do not participate in the Néel transition (which is not surprising because of the classical nature of the finite-temperature phase transition).

The asymptotic exponential decay is clearly exhibited by $C_{\text{tot}}(i, j)$ for $T > T_N$ and distances exceeding a few lattice steps. The spatial structure of the quantum covariance is generally more complex (see Appendix B for an extended discussion); however, a first exponential decay sets in after a few lattice steps, and this decay is clearly visible in the experimental data. We shall focus on the length associated with this short-range decay in the following and extract it via a linear-regression (LR) estimator $\xi_{Q,\text{LR}}$ from a linear fit of the logarithm of the correlation function or via a second-moment estimator $\xi_{Q,2}$ (see the next section). Figure 3(a) shows the LR estimators for ξ and ξ_Q , comparing experiment and numerical

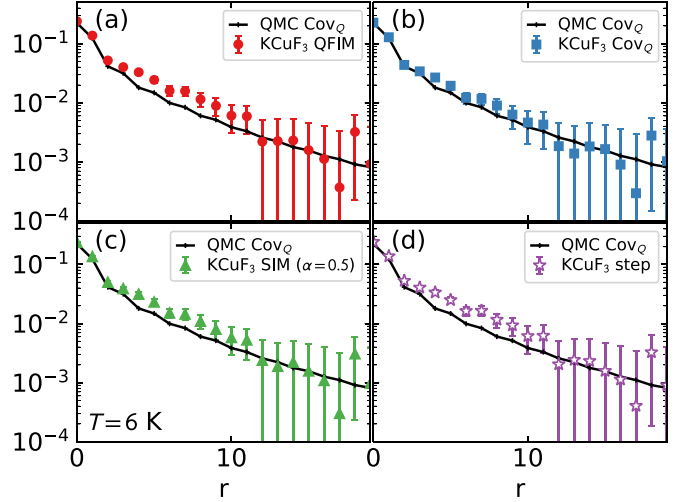


FIG. 4. Various quantum correlation functions evaluated for KCuF_3 at 6 K. (a) The quantum Fisher information matrix [Eq. (3)], scaled as $\text{QFIM}/4$. (b) The quantum covariance Cov_Q [Eq. (5)]. (c) The skew information matrix [SIM; Eq. (7)]. (d) Correlation function using the simple filter $h^{\text{step}}(x)$ [Eq. (10)]. In all panels the experimental data are compared with the QMC data for Cov_Q for reference. The error bars represent one standard deviation uncertainty.

simulations and exposing the large difference between the two length scales.

One may wonder how the spatial extension of quantum correlations relates to multipartite entanglement, namely, the entanglement depth. In fact, there is a rigorous relationship: the entanglement depth along the chains is bounded from below by the Var_Q density or the QFI density for the staggered magnetization $M_s = \sum_r (-1)^r S_i^z$ of the individual chains, namely, $\text{Var}_Q(M_{s,\text{chain}})/N = \sum_r (-1)^r \text{Cov}_Q(i, i+r)$ and $\text{QFI}(M_{s,\text{chain}})/N = \sum_r (-1)^r \text{QFIM}(i, i+r)$, where r runs over distances along the chains. Indeed, when $4\text{Var}_Q/N > k$ or when $\text{QFI}/N > k$, one can conclude that spins in each chain exhibit at least $(k+1)$ -partite entanglement [17,42,43]. Figure 3(b) shows the temperature dependence of 4Var_Q and QFI for KCuF_3 compared with the theoretical results for 4Var_Q . Interestingly, the entanglement depth estimate offered by these quantities is comparable to the quantum coherence length, rising up to $k+1 = 4$. In general, one should expect quantum correlations to be systematically longer ranged than the depth of entanglement, given that entanglement is a stronger form of correlation and a state can be quantum correlated without being entangled [12].

The various quantum correlation functions offered by Eq. (1) raise the question of whether the quantum coherence length is uniquely defined or depends on the quantum filter h . Figure 4 shows that the same exponential decay is exhibited by all quantum correlation functions listed above (Cov_Q , QFIM, SIM). In fact, it is a rather robust feature, uniquely stemming from the high-pass nature of $h(x)$. To emphasize the universality, we also calculate the most naive correlation $C[O_i, O_j; h^{\text{step}}, \rho]$ using a step function filter:

$$h^{\text{step}}(x) = \begin{cases} 1 & \text{if } x/2 \geq 1, \\ 0 & \text{if } x/2 < 1 \end{cases} \quad (10)$$

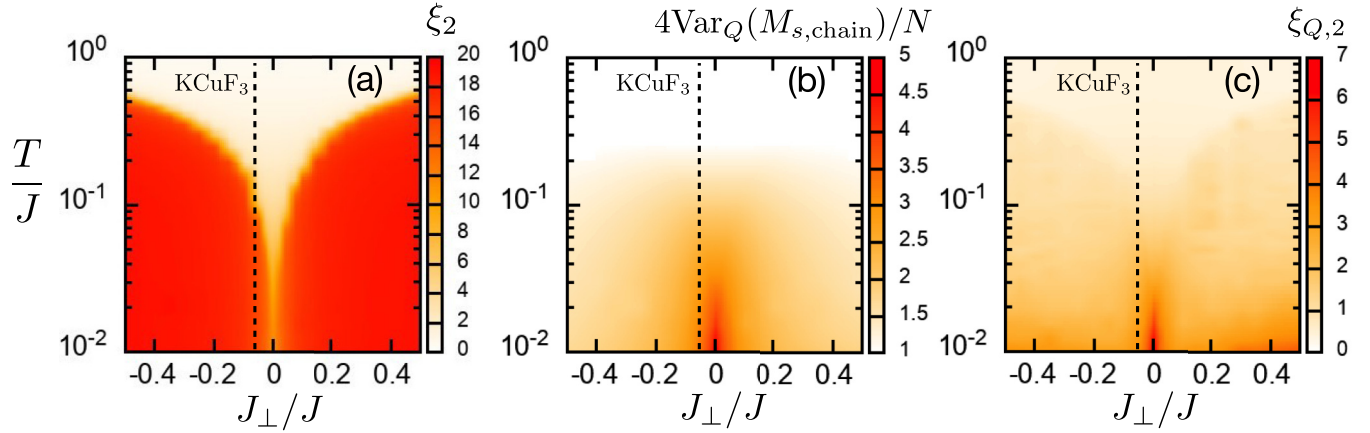


FIG. 5. Total vs quantum correlations for coupled Heisenberg chains from QMC data. (a) Second-moment estimator for the in-chain correlation length ξ_2 , clearly showing the Néel order. (b) Quantum variance per spin of the in-chain staggered magnetization, $4\text{Var}_Q(M_s)/N$. (c) Second-moment estimator for the in-chain quantum coherence length $\xi_{Q,2}$. In all panels, the dashed line marks the value of J_\perp/J realized by KCuF_3 .

in Eq. (1), such that all intensity below $\hbar\omega/2k_B T$ is suppressed. Although this filter function lacks the linear behavior at small x required for a proper quantum coherence measure, the plot in Fig. 4(d) shows the same general behavior as the other quantum correlators. (Furthermore, the step function resembles filter functions that are naturally applied in neutron scattering experiments; see the discussion below.) Thus, although the details of the quantum correlators depend on the filter function, the revealed length scale appears to be universal. The temperature dependence of all four quantum correlators is shown in Appendix C.

V. REDISTRIBUTION OF QUANTUM CORRELATIONS UPON CHANGING THE INTERCHAIN COUPLINGS

We now embed the quantum correlations in KCuF_3 within the broader family of coupled spin chain models described by the Hamiltonian (8). Using QMC simulations, we calculate correlations and quantum coherence with varying interchain coupling J_\perp in order to explore the effect of the dimensionality of interactions. In the case of total correlations, an increase in $|J_\perp|$ at fixed temperature drives the system from quasi-one-dimensional magnetism towards three-dimensional magnetism, i.e., towards a regime exhibiting stronger correlations in *all* spatial directions, both transverse and longitudinal to the chains. This behavior is clearly exhibited by the second-moment estimator for the in-chain correlation length

$$\xi_2^2 = \frac{1}{2} \frac{\sum_r r^2 |\langle \mathbf{S}_i \cdot \mathbf{S}_{i+r} \rangle|}{\sum_r |\langle \mathbf{S}_i \cdot \mathbf{S}_{i+r} \rangle|}, \quad (11)$$

which allows for a systematic extraction of a typical length from all the correlation data produced with QMC across the vast parameter range explored in Fig. 5. As shown in Fig. 5(a), the total second-moment estimator's sharp rise upon lowering the temperature marks the evolution of the Néel temperature with the interchain coupling [44].

On the other hand, quantum correlations are found to undergo a rather different fate along the dimensional crossover of the couplings. Figures 5(b) and 5(c) show the T and J_\perp dependence of $\xi_{Q,2}$ [defined analogously to Eq. (11) by

substituting $|\langle \mathbf{S}_i \cdot \mathbf{S}_{i+r} \rangle|$ with $\text{Cov}_Q(i, i+r)$ and $\text{Var}_Q(M_{s,\text{chain}})/N$ (a lower bound on the in-chain entanglement depth). In contrast to total correlations, quantum correlations along the chains appear to *decrease* upon increasing the interchain couplings at low T (and the Néel transition is nearly invisible to $\text{Var}_Q(M_{s,\text{chain}})/N$; see Ref. [33] for further details on this aspect). The quantum coherence length ξ_Q is, in fact, found to increase again at sufficiently low temperature and sufficiently strong J_\perp , but this is an effect driven by the appearance of thin tails in the quantum correlation function which have little effect on the integral given by the quantum variance (Appendix B).

This result suggests that low-temperature quantum correlations in coupled-chain systems exhibit a form of *monogamy* [45] since a dimensional crossover in the couplings entails their spatial redistribution from in-chain to interchain correlations. This result is quite insightful. In general, quantum correlations are not necessarily monogamous, as they can also be associated with states possessing multipartite entanglement, which can imply an arbitrary number of degrees of freedom. The above behavior suggests that the Heisenberg two-spin couplings are primarily promoting quantum correlations in the form of two-spin entanglement, presumably via singlet and triplet formation for antiferromagnetic and ferromagnetic couplings, respectively, which is indeed monogamous [45,46]. As a result, quantum correlations along the chains decrease over shorter length scales when the interchain coupling is increased. This result shows that, among the family of coupled-chain Heisenberg models, quasi-one-dimensional compounds such as KCuF_3 exhibit the strongest quantum correlations at short distance, whose detection via neutron scattering is most efficient. (In Appendix B we also show that interchain quantum correlations do not rise to the same strength as that of intrachain ones over the range of interchain couplings explored in this study.)

VI. DISCUSSION

These results have exciting implications far beyond one-dimensional (1D) spin chains. First, our results on 1D

chains demonstrate that the spatial structure of quantum correlations reveals new *quantitative* information about the dimensionality of quantum materials, a fundamental property inherently linked to quantum statistics and novel phases of matter. This is important as “low-dimensional materials” often exist in a three-dimensional host crystal and retain weak three-dimensional coupling. Our methods give access to the effective dimensionalities of both quantum and total correlations, which may be rather different, as our results clearly show. In this respect, it is important to note that our quantum correlator analysis is not restricted to neutron spectroscopy: any momentum-resolved probe of dynamic susceptibility associated with local Hermitian operators will work in the same fashion. For instance, quantum correlations in the charge sector could be probed via x-ray scattering [47] or electron energy-loss spectroscopy [48], offering complementary pictures of quantum coherence in a huge variety of quantum materials.

Second, the quantum correlators are model independent, which allows precise statements to be made about materials even in the absence of a tractable theory. Therefore, they may yield important information about enigmatic condensed matter states. For example, one could evaluate how the spatial structure of quantum correlations changes across quantum phase transitions (as in, e.g., heavy fermion materials [49] and quantum magnets under fields). Recent works [18,50] showed that quantum correlations can reconstruct the quantum critical fan occurring at finite temperatures above such quantum critical points, thus certifying quantum criticality and delineating the range of genuine quantum critical behavior. Within the space of coupled spin chains, it would be interesting to apply the same analysis to systems with frustrated interchain coupling, such as Cs_2CuCl_4 [51,52], in order to test whether frustration can stabilize the intrachain quantum coherence length compared to the unfrustrated case studied here.

Third, more generally, our results advance the synthesis of condensed matter physics and quantum information. Specifically, we show that experimental momentum-resolved dynamical response functions at thermal equilibrium can be mined for a wealth of many-body quantum information. The ability to do this for a thermodynamic system at a well-defined temperature is not shared by many other platforms for quantum many-body physics. (For example, most quantum many-body physics simulators based on atomic physics platforms do not operate at thermal equilibrium, or if they do, their temperature is not easily accessible or cannot easily be held fixed [53–55]. As a consequence, an analysis similar to ours cannot be straightforwardly conducted with, e.g., cold atoms.) Hence, our results indicate a clear path for experiments on quantum materials to positively contribute to quantum information theory by revealing the microscopic structure of quantum correlations in many-body states.

We also note that quantum correlations can be extracted without Fourier transforming the momentum-resolved spectroscopic data. If the integral over frequencies defining quantum correlations in Eq. (1) is carried out using $\chi''(\mathbf{Q}, \omega)$, one can extract a quantum structure factor and hence a quantum coherence length by fitting the structure factor to a resolution-convolved Lorentzian in a way analogous to how total correlations are conventionally extracted from

energy-integrated Bragg peaks. Although much information about the detailed spatial dependence of quantum correlations is lost using this procedure, it may prove an easier experimental way to evaluate a quantum coherence length in higher-dimensional materials.

On a different note, the fact that the step function filter captures the same behavior as the other quantum correlators suggests that approximate results for the quantum length scale can be experimentally obtained by neutron diffraction methods. At low temperatures where $\chi''(\mathbf{k}, \omega) \approx \pi S(\mathbf{k}, \omega)$, the filter function $h^{\text{step}}(x)$ can be traded for a physical neutron transmission filter (e.g., beryllium powder) [56,57], tuning the incident neutron energy to act as a high-pass filter in energy transfer $\hbar\omega$ (absorbing neutrons with large final energy). For suitable systems (specifically, low-bandwidth materials such as $\text{CuSO}_4 \cdot 5\text{D}_2\text{O}$ [58], YbAlO_3 [59], and Cs_2CoCl_4 [21]) it offers a path to quickly identifying whether a material has significant quantum correlations.

VII. CONCLUSIONS

We showed how the spatial structure of quantum correlation functions for quantum spin systems can be extracted from neutron spectroscopy data. The data revealed the existence of a fundamental length scale of quantum mechanical origin—the quantum coherence length—limiting the range of quantum correlations at all finite temperatures, which is wildly different from the correlation length. Our study also highlighted the role of dimensionality on quantum correlations, showing that a stronger coupling between Heisenberg chains leads to a redistribution of quantum correlations from the chains to the transverse directions, in contrast to total correlations. As a consequence, within the family of coupled-chain compounds, systems close to the one-dimensional limit, such as KCuF_3 , exhibit the strongest short-range quantum correlations and the weakest total correlations. The fact that quantum correlators enabled new observations—even for a well-studied model like the one-dimensional Heisenberg chain—indicates that quantum correlator analysis could be a powerful new way of assessing the underlying quantum state of a vast number of quantum materials, both low- and higher-dimensional.

ACKNOWLEDGMENTS

We thank I. Frérot for valuable discussions. The work by A.S. and D.A.T. is supported by the Quantum Science Center (QSC), a National Quantum Information Science Research Center of the U.S. Department of Energy (DOE). The work of P.L. and E.D. was supported by the U.S. Department of Energy, Office of Science, Basic Energy Sciences, Materials Sciences and Engineering Division. All QMC calculations were performed on the PSMN cluster at the ENS of Lyon.

APPENDIX A: EXPERIMENTAL DATA PROCESSING

The explicit data analysis protocol for extracting real space quantum correlators is as follows:

- (1) Isolate magnetic scattering in a full Brillouin zone.
- (2) Correct for the form factor and g factor.

(3) Correct for the polarization factor (if anisotropic exchange exists).

(4) Normalize data to absolute units and convert to χ'' [60].

(5) Take the Fourier transform from reciprocal to real space.

(6) Apply the filter function h .

(7) Analyze the spatial dependence.

Note that steps 5 and 6 can be exchanged for equivalent results. Note also that step 3 is necessary only if anisotropy is present such that $S_{xx} \neq S_{yy} \neq S_{zz}$, in which case one must correct for the experimental neutron polarization factor [40]. This can be done with theoretical modeling [21] or more generally by measuring polarized neutron scattering. In this study, we used a highly isotropic system, and thus, step 3 was not necessary.

All experimental data used in this study were previously published in [37], which involved a composite dataset from two different neutron experiments for temperatures $T = 75$ K and above: SEQUOIA at the Spallation Neutron Source [61] for low energy and MAPS at ISIS [62] for high energy. The data at $T = 6$ K and 50 K are from ISIS. For the quantum correlators, we applied the formulas to the data as previously processed. However, for the conventional correlation length at $T = 6$ K, we applied a resolution deconvolution. This is because KCuF_3 at $T = 6$ K has long-range magnetic order and a very long correlation length (~ 700 sites [63]). Consequently, resolution broadening has to be corrected before the true long-range correlations will emerge. We did this by fitting the $q = \pi$, $T = 6$ K, $\hbar\omega = 0$ scattering to a Gaussian function and dividing the Fourier transformed structure factor by the Fourier transformed Gaussian function. This resulted in a visible increase in total correlations for $r > 15$. For only the $T = 6$ K conventional correlations did this correction make any visible difference.

It should be noted that the experimental energy and momentum resolution limit how low in temperature and how far in real space one can analyze the quantum correlations. As the resolution of each improves, one can evaluate lower temperatures and larger spatial distances. Although the limits of each is not something we explore in this paper, one can still use resolution as a rough guideline: if $\Delta\hbar\omega$ is the energy resolution, one can only be sensitive to temperatures such that $k_B T > \Delta\hbar\omega$, and one cannot fully appreciate the enhancement of quantum correlations when cooling below this temperature scale. Similarly, if ΔQ is the average momentum resolution along a particular reciprocal space direction, one can only evaluate distances $\leq \frac{2\pi}{\Delta Q}$ along that direction in real space.

APPENDIX B: EVOLUTION OF QUANTUM CORRELATIONS UPON CHANGING THE INTERCHAIN COUPLINGS

Here we discuss the detailed evolution of the spatial structure of quantum correlations upon changing the strength of the coupling between Heisenberg chains, calculated from our experimental and theoretical data. Figure 6 shows a comparison between the experimental data for two different quantum correlation functions (quantum covariance and the quantum Fisher information matrix) for KCuF_3 at $T = 6$ K and

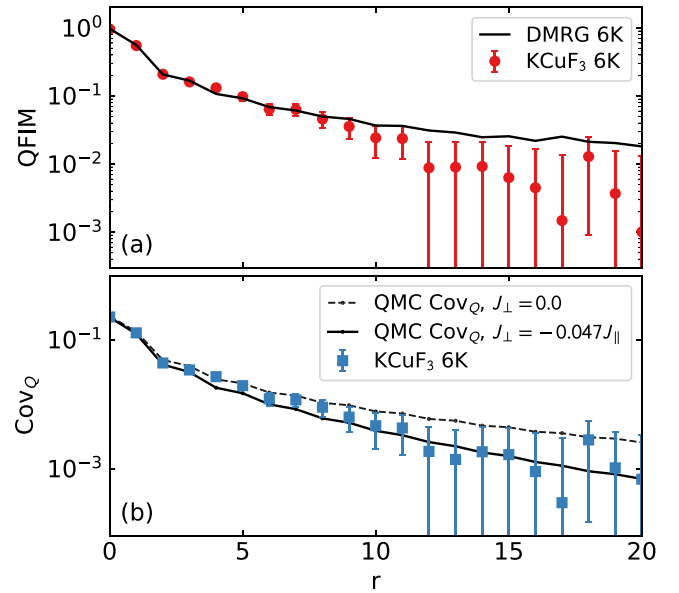


FIG. 6. Comparison between (a) 1D theoretical QFIM and (b) quantum covariance and experimental KCuF_3 data at 6 K. For comparison, the QMC result for KCuF_3 J_{\perp} is also shown in (b). Note that the $r > 10$ experimental values are systematically smaller than the theoretical 1D calculations as a consequence of finite interchain coupling J_{\perp} .

theoretical data obtained for a single one-dimensional chain. In particular the theory data for quantum covariance are obtained via quantum Monte Carlo (QMC) as in the main text. On the other hand, the data for the quantum Fisher information matrix are inaccessible to QMC because they require full knowledge of the dynamical susceptibility. For one-dimensional systems, this knowledge can be obtained using the density-matrix renormalization group (DMRG) [64,65], which allows for the calculation of $S(k, \omega)$ at finite temperature [66,67]. Here we extend the finite- T calculations reported in Ref. [20] down to $T = 6$ K. We use the DMRG++ software [68] to study a system with open boundary conditions consisting of $L = 50$ physical sites and 50 “ancilla” sites. $S(k, \omega)$ spectra are calculated using the Krylov-space correction vector method [69,70], with a Lorentzian energy broadening with half width at half maximum $\eta = 0.1J$. For details on how to reproduce the DMRG calculations, see the Supplemental Material of Ref. [20].

As seen in Fig. 6, the predictions for the quantum correlation functions of a single one-dimensional chain lie systematically above the measured values for KCuF_3 , while a much better quantitative agreement is obtained when taking into account the small, albeit finite, interchain coupling J_{\perp} , as shown in Fig. 6(b). This indicates that (1) the resolution of the experiment is clearly sufficient to reconstruct the difference between isolated and weakly coupled Heisenberg chains and (2) moving from a single chain to coupled chains, quantum correlations reorganize spatially in such a way that correlations along the chains are suppressed.

We examine this trend systematically via QMC by monitoring how the spatial structure of the quantum covariance changes upon increasing the magnitude of the

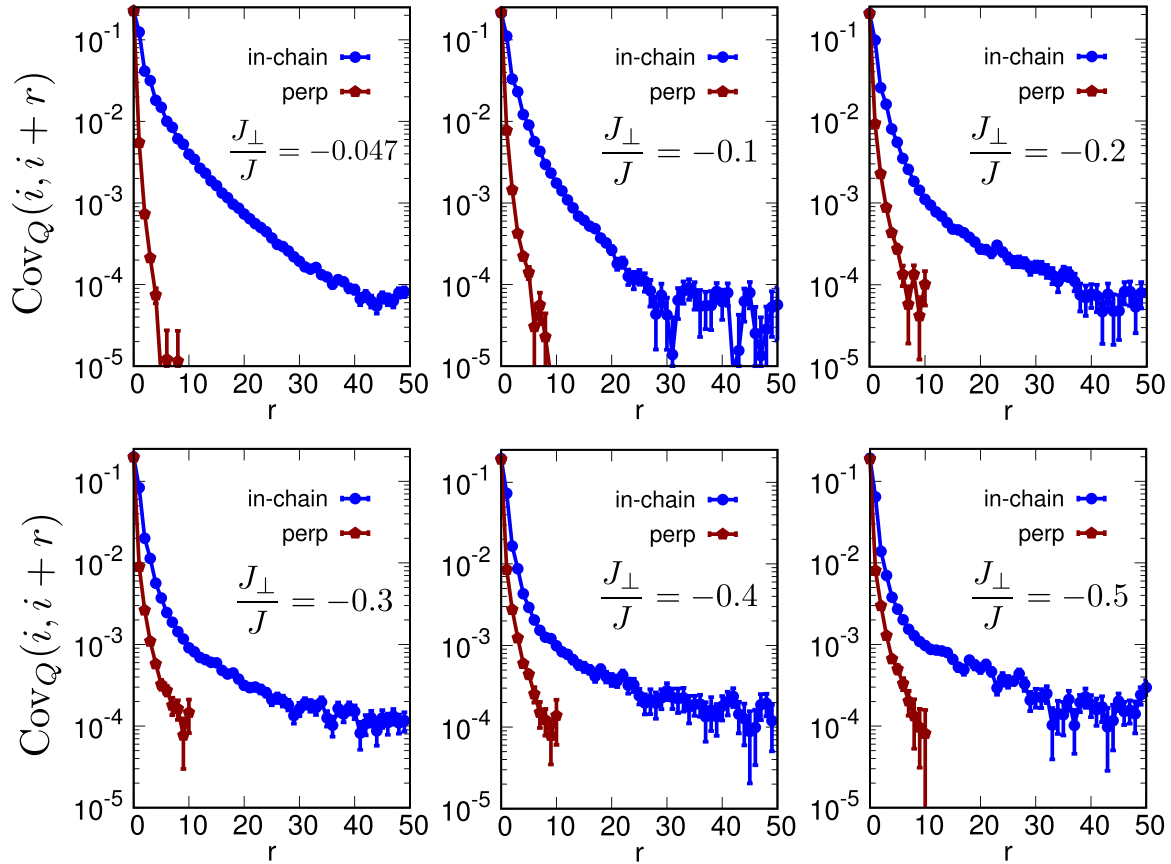


FIG. 7. Dependence of Cov_Q on J_\perp . Dependence of the quantum covariance on the ferromagnetic interchain coupling J_\perp for $J_\perp/J = -0.047$ (like for KCuF_3), -0.1 , -0.2 , -0.3 , -0.4 , and -0.5 at a temperature $T/k_B = 6J/388$ (corresponding to 6 K for KCuF_3). The panels show QMC data obtained for a system with a size of $100 \times 20 \times 20$. Each panel shows the in-chain correlations [$\text{Cov}_Q(i, i+x)$, taking x as the lattice direction parallel to the chains] and the correlations perpendicular to the chain [e.g., $\text{Cov}_Q(i, i+y)$].

ferromagnetic coupling ($J_\perp < 0$) between the chains. In particular we examine the quantum covariance at $T = 6$ K (assuming an in-chain coupling equal to that of KCuF_3) along the chains, namely, $\text{Cov}_Q(i, i+x)$, taking x as the direction of extension of the chains, and perpendicular to the chains, namely, $\text{Cov}_Q(i, i+y)$, where y is one of the two perpendicular lattice directions. Figure 7 shows that, upon increasing $|J_\perp|$, the correlations along a coordinate axis perpendicular to the chain become stronger, as can be trivially expected, although they remain much weaker than the in-chain correlations for the whole range of values of J_\perp we explored ($|J_\perp| \leq J/2$). On the other hand, the in-chain quantum covariance undergoes a much more complex evolution: it becomes significantly weaker at short range when $|J_\perp|$ increases, witnessing a form of monogamy of short-range quantum correlations, as discussed in the main text. Yet the behavior at long range shows an opposite trend for sufficiently large $|J_\perp|$, as the in-chain quantum covariance develops a stronger tail. This tail can be associated with the appearance of long-range *multipartite* quantum correlations. Such correlations are expected in a long-range-ordered quantum ground state, such as that of a system of coupled Heisenberg chains, and their multipartite nature causes them to no longer be monogamous. Nonetheless, the long-range tail is rather thin, and it makes a small contribution to the quantum variance of the in-chain

staggered magnetization, so that the global trend is a decrease in this quantity with $|J_\perp|$, as shown in Fig. 5(b) of the main text.

The buildup of increasingly strong multipartite quantum correlations and entanglement upon coupling the chains is clearly exhibited in Fig. 8, in which the quantum variance density of the order parameter $M_{\mathbf{Q}} = \sum_i e^{i\mathbf{Q}\cdot\mathbf{r}_i} S_i^z$ is shown; the ordering vector \mathbf{Q} is $(\pi, 0, 0)$ for $J_\perp < 0$ and (π, π, π) for $J_\perp = 0$. We clearly observe that rather massive entanglement sets in at low temperatures in the more strongly coupled chains, involving >40 spins within the temperature and parameter range we explored. Yet this behavior really stems from the buildup of correlations transverse to the chains, as can easily be deduced by making a comparison with Fig. 5(b) of the main text.

APPENDIX C: COMPARING QUANTUM CORRELATORS

For a comparison of the experimental and theoretical quantum correlators at all measured temperatures, see Fig. 9. Note that above $T = 75$ K, only a few nearest neighbors have quantum correlations distinguishable from the large r background noise. This is a consequence of the experimental background in KCuF_3 , which was previously discussed in Ref. [20].

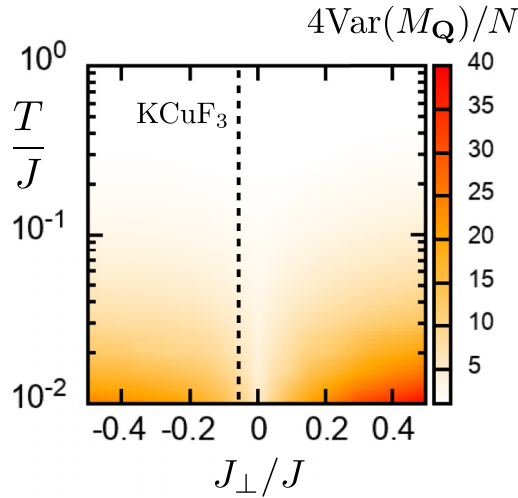


FIG. 8. Quantum variance density of the order parameter for coupled Heisenberg chains. The ordering vector \mathbf{Q} is $(\pi, 0, 0)$ for $J_{\perp} < 0$ and (π, π, π) for $J_{\perp} = 0$.

The DMRG data for the QFIM on isolated chains at finite temperature, shown in Fig. 9, may erroneously suggest that the latter quantity possesses a decay length which is systematically larger than that of, e.g., Cov_Q . This discrepancy is, in fact, not intrinsic; it is, rather, the result of the fact that the DMRG calculations are done on isolated chains, while the theoretical curves for Cov_Q are QMC data for coupled chains. Indeed, as noted in the main text, the strength of the interchain coupling J_{\perp} makes a dramatic difference in the length scale of

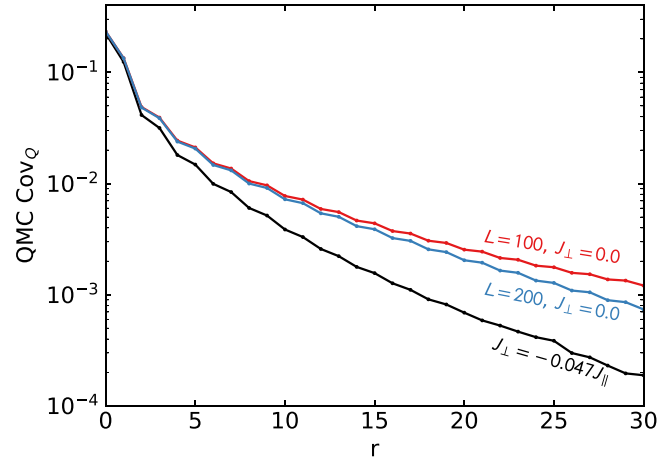


FIG. 10. Quantum covariance from quantum Monte Carlo (QMC) for coupled and uncoupled chains. The quantum covariance is much longer ranged in the one-dimensional $J_{\perp} = 0$ limit. Meanwhile, the chain length slightly decreases the length scale, in accord with the periodic boundary being farther away.

the quantum correlator. Figure 10 shows this more explicitly, with Cov_Q plotted for the KCuF_3 value of J_{\perp} and for $J_{\perp} = 0$. See also the detailed discussion of this topic in Appendix B.

In the case of one-dimensional QMC simulations, we also show a comparison of the quantum covariances for two different system sizes ($L = 100$ and $L = 200$). The data display minor differences over the range of distances which are relevant for the experiment. We therefore conclude that the QMC data we use for the quantum covariance are essentially devoid of significant finite-size effects.

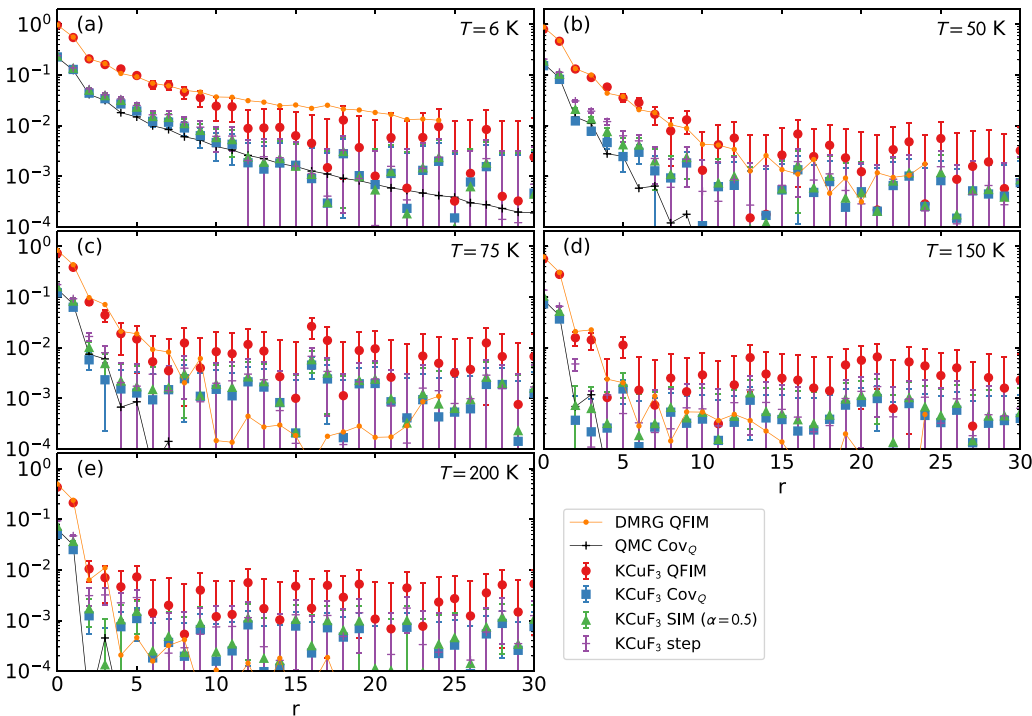


FIG. 9. Full temperature dependence of the quantum correlation functions. Absolute values of various definitions of the quantum correlator applied to KCuF_3 at temperatures between $T = 6$ K and $T = 200$ K, as well as QMC and DMRG calculations for comparison. (a) corresponds to Fig. 4 in the main text, but with the raw values of the QFI matrix.

- [1] R. Horodecki, P. Horodecki, M. Horodecki, and K. Horodecki, Quantum entanglement, *Rev. Mod. Phys.* **81**, 865 (2009).
- [2] N. Brunner, D. Cavalcanti, S. Pironio, V. Scarani, and S. Wehner, Bell nonlocality, *Rev. Mod. Phys.* **86**, 419 (2014).
- [3] X.-L. Wang, L.-K. Chen, W. Li, H.-L. Huang, C. Liu, C. Chen, Y.-H. Luo, Z.-E. Su, D. Wu, Z.-D. Li, H. Lu, Y. Hu, X. Jiang, C.-Z. Peng, L. Li, N.-L. Liu, Y.-A. Chen, C.-Y. Lu, and J.-W. Pan, Experimental ten-photon entanglement, *Phys. Rev. Lett.* **117**, 210502 (2016).
- [4] P. Thomas, L. Ruscio, O. Morin, and G. Rempe, Efficient generation of entangled multiphoton graph states from a single atom, *Nature (London)* **608**, 677 (2022).
- [5] T. Monz, P. Schindler, J. T. Barreiro, M. Chwalla, D. Nigg, W. A. Coish, M. Harlander, W. Hänsel, M. Hennrich, and R. Blatt, 14-qubit entanglement: Creation and coherence, *Phys. Rev. Lett.* **106**, 130506 (2011).
- [6] R. Schmied, J.-D. Bancal, B. Allard, M. Fadel, V. Scarani, P. Treutlein, and N. Sangouard, Bell correlations in a Bose-Einstein condensate, *Science* **352**, 441 (2016).
- [7] A. Omran, H. Levine, A. Keesling, G. Semeghini, T. T. Wang, S. Ebadi, H. Bernien, A. S. Zibrov, H. Pichler, S. Choi, J. Cui, M. Rossignolo, P. Rembold, S. Montangero, T. Calarco, M. Endres, M. Greiner, V. Vuletić, and M. D. Lukin, Generation and manipulation of Schrödinger cat states in Rydberg atom arrays, *Science* **365**, 570 (2019).
- [8] C. Song, K. Xu, H. Li, Y.-R. Zhang, X. Zhang, W. Liu, Q. Guo, Z. Wang, W. Ren, J. Hao, H. Feng, H. Fan, D. Zheng, D.-W. Wang, H. Wang, and S.-Y. Zhu, Generation of multicomponent atomic Schrödinger cat states of up to 20 qubits, *Science* **365**, 574 (2019).
- [9] G. J. Mooney, C. D. Hill, and L. C. L. Hollenberg, Entanglement in a 20-qubit superconducting quantum computer, *Sci. Rep.* **9**, 13465 (2019).
- [10] B. Keimer and J. Moore, The physics of quantum materials, *Nat. Phys.* **13**, 1045 (2017).
- [11] Y. Tokura, M. Kawasaki, and N. Nagaosa, Emergent functions of quantum materials, *Nat. Phys.* **13**, 1056 (2017).
- [12] G. Adesso, T. R. Bromley, and M. Cianciaruso, Measures and applications of quantum correlations, *J. Phys. A* **49**, 473001 (2016).
- [13] G. D. Chiara and A. Sanpera, Genuine quantum correlations in quantum many-body systems: a review of recent progress, *Rep. Prog. Phys.* **81**, 074002 (2018).
- [14] L. Pezzè, A. Smerzi, M. K. Oberthaler, R. Schmied, and P. Treutlein, Quantum metrology with nonclassical states of atomic ensembles, *Rev. Mod. Phys.* **90**, 035005 (2018).
- [15] I. Frérot, M. Fadel, and M. Lewenstein, Probing quantum correlations in many-body systems: a review of scalable methods, *Rep. Prog. Phys.* **86**, 114001 (2023).
- [16] P. Hauke, M. Heyl, L. Tagliacozzo, and P. Zoller, Measuring multipartite entanglement through dynamic susceptibilities, *Nat. Phys.* **12**, 778 (2016).
- [17] I. Frérot and T. Roscilde, Quantum variance: A measure of quantum coherence and quantum correlations for many-body systems, *Phys. Rev. B* **94**, 075121 (2016).
- [18] I. Frérot and T. Roscilde, Reconstructing the quantum critical fan of strongly correlated systems using quantum correlations, *Nat. Commun.* **10**, 577 (2019).
- [19] G. Mathew, S. L. L. Silva, A. Jain, A. Mohan, D. T. Adroja, V. G. Sakai, C. V. Tomy, A. Banerjee, R. Goret, Aswathi V. N., R. Singh, and D. Jaiswal-Nagar, Experimental realization of multipartite entanglement via quantum Fisher information in a uniform antiferromagnetic quantum spin chain, *Phys. Rev. Res.* **2**, 043329 (2020).
- [20] A. Scheie, P. Laurell, A. M. Samarakoon, B. Lake, S. E. Nagler, G. E. Granroth, S. Okamoto, G. Alvarez, and D. A. Tennant, Witnessing entanglement in quantum magnets using neutron scattering, *Phys. Rev. B* **103**, 224434 (2021).
- [21] P. Laurell, A. Scheie, C. J. Mukherjee, M. M. Koza, M. Enderle, Z. Tylczynski, S. Okamoto, R. Coldea, D. A. Tennant, and G. Alvarez, Quantifying and controlling entanglement in the quantum magnet Cs_2CoCl_4 , *Phys. Rev. Lett.* **127**, 037201 (2021).
- [22] S. L. Braunstein and C. M. Caves, Statistical distance and the geometry of quantum states, *Phys. Rev. Lett.* **72**, 3439 (1994).
- [23] A. O. Scheie, E. A. Ghioldi, J. Xing, J. A. M. Paddison, N. E. Sherman, M. Dupont, L. D. Sanjeeva, S. Lee, A. J. Woods, D. Abernathy *et al.*, Proximate spin liquid and fractionalization in the triangular antiferromagnet KYbSe_2 , *Nat. Phys.* **20**, 74 (2024).
- [24] B. Lake, D. A. Tennant, C. D. Frost, and S. E. Nagler, Quantum criticality and universal scaling of a quantum antiferromagnet, *Nat. Mater.* **4**, 329 (2005).
- [25] B. Lake, D. A. Tennant, J.-S. Caux, T. Barthel, U. Schollwöck, S. E. Nagler, and C. D. Frost, Multispinon continua at zero and finite temperature in a near-ideal Heisenberg chain, *Phys. Rev. Lett.* **111**, 137205 (2013).
- [26] D. Malpetti and T. Roscilde, Quantum correlations, separability, and quantum coherence length in equilibrium many-body systems, *Phys. Rev. Lett.* **117**, 130401 (2016).
- [27] T. Kuwahara and K. Saito, Exponential clustering of bipartite quantum entanglement at arbitrary temperatures, *Phys. Rev. X* **12**, 021022 (2022).
- [28] E. P. Wigner and M. M. Yanase, Information contents of distributions, *Proc. Natl. Acad. Sci. USA* **49**, 910 (1963).
- [29] D. Forster, *Hydrodynamic Fluctuations, Broken Symmetry, and Correlation Functions*, Advanced Book Classics (Westview Press, Boulder Colorado, 1995).
- [30] D. Petz, Monotone metrics on matrix spaces, *Linear Algebra Appl.* **244**, 81 (1996).
- [31] P. Gibilisco, D. Imparato, and T. Isola, Inequalities for quantum Fisher information, *Proc. Am. Math. Soc.* **137**, 317 (2009).
- [32] I. Frérot, A quantum statistical approach to quantum correlations in many-body systems, Ph.D. thesis, École normale supérieure de Lyon, 2017.
- [33] I. Frérot, A. Raçon, and T. Roscilde, Thermal critical dynamics from equilibrium quantum fluctuations, *Phys. Rev. Lett.* **128**, 130601 (2022).
- [34] J. Liu, H. Yuan, X.-M. Lu, and X. Wang, Quantum Fisher information matrix and multiparameter estimation, *J. Phys. A* **53**, 023001 (2020).
- [35] M. Jarrell and J. Gubernatis, Bayesian inference and the analytic continuation of imaginary-time quantum Monte Carlo data, *Phys. Rep.* **269**, 133 (1996).
- [36] S. Lovesey, *Theory of Neutron Scattering from Condensed Matter* (Clarendon, Oxford, 1984).
- [37] A. Scheie, P. Laurell, B. Lake, S. E. Nagler, M. B. Stone, J.-S. Caux, and D. A. Tennant, Quantum wake dynamics in Heisenberg antiferromagnetic chains, *Nat. Commun.* **13**, 5796 (2022).

- [38] D. A. Tennant, T. G. Perring, R. A. Cowley, and S. E. Nagler, Unbound spinons in the $S = 1/2$ antiferromagnetic chain KCuF_3 , *Phys. Rev. Lett.* **70**, 4003 (1993).
- [39] B. Lake, D. A. Tennant, and S. E. Nagler, Longitudinal magnetic dynamics and dimensional crossover in the quasi-one-dimensional spin- $\frac{1}{2}$ Heisenberg antiferromagnet KCuF_3 , *Phys. Rev. B* **71**, 134412 (2005).
- [40] G. L. Squires, *Introduction to the Theory of Thermal Neutron Scattering*, 3rd ed. (Cambridge University Press, Cambridge, 2012).
- [41] O. F. Syljuåsen and A. W. Sandvik, Quantum Monte Carlo with directed loops, *Phys. Rev. E* **66**, 046701 (2002).
- [42] P. Hyllus, W. Laskowski, R. Krischek, C. Schwemmer, W. Wiczcok, H. Weinfurter, L. Pezzé, and A. Smerzi, Fisher information and multiparticle entanglement, *Phys. Rev. A* **85**, 022321 (2012).
- [43] G. Tóth, Multipartite entanglement and high-precision metrology, *Phys. Rev. A* **85**, 022322 (2012).
- [44] C. Yasuda, S. Todo, K. Hukushima, F. Alet, M. Keller, M. Troyer, and H. Takayama, Néel temperature of quasi-low-dimensional Heisenberg antiferromagnets, *Phys. Rev. Lett.* **94**, 217201 (2005).
- [45] V. Coffman, J. Kundu, and W. K. Wootters, Distributed entanglement, *Phys. Rev. A* **61**, 052306 (2000).
- [46] T. J. Osborne and F. Verstraete, General monogamy inequality for bipartite qubit entanglement, *Phys. Rev. Lett.* **96**, 220503 (2006).
- [47] W. Schülke, *Electron Dynamics by Inelastic X-ray Scattering*, Oxford Series on Synchrotron Radiation (Oxford University Press, Oxford, 2007), Vol. 7.
- [48] S. Vig, A. Kogar, M. Mitrano, A. A. Husain, V. Mishra, M. S. Rak, L. Venema, P. D. Johnson, G. D. Gu, E. Fradkin, M. R. Norman, and P. Abbamonte, Measurement of the dynamic charge response of materials using low-energy, momentum-resolved electron energy-loss spectroscopy (M-EELS), *SciPost Phys.* **3**, 026 (2017).
- [49] P. Gegenwart, Q. Si, and F. Steglich, Quantum criticality in heavy-fermion metals, *Nat. Phys.* **4**, 186 (2008).
- [50] M. Gabbriellini, A. Smerzi, and L. Pezzè, Multipartite entanglement at finite temperature, *Sci. Rep.* **8**, 15663 (2018).
- [51] R. Coldea, D. A. Tennant, K. Habicht, P. Smeibidl, C. Wolters, and Z. Tylczynski, Direct measurement of the spin Hamiltonian and observation of condensation of magnons in the 2D frustrated quantum magnet Cs_2CuCl_4 , *Phys. Rev. Lett.* **88**, 137203 (2002).
- [52] O. A. Starykh, H. Katsura, and L. Balents, Extreme sensitivity of a frustrated quantum magnet: Cs_2CuCl_4 , *Phys. Rev. B* **82**, 014421 (2010).
- [53] D. C. McKay and B. DeMarco, Cooling in strongly correlated optical lattices: Prospects and challenges, *Rep. Prog. Phys.* **74**, 054401 (2011).
- [54] S. Trotzky, L. Pollet, F. Gerbier, U. Schnorrberger, I. Bloch, N. V. Prokof'ev, B. Svistunov, and M. Troyer, Suppression of the critical temperature for superfluidity near the Mott transition, *Nat. Phys.* **6**, 998 (2010).
- [55] C. Carcy, G. Hercé, A. Tenart, T. Roscilde, and D. Clément, Certifying the adiabatic preparation of ultracold lattice bosons in the vicinity of the Mott transition, *Phys. Rev. Lett.* **126**, 045301 (2021).
- [56] P. Egelstaff and R. Pease, The design of cold neutron filters, *J. Sci. Instrum.* **31**, 207 (1954).
- [57] D. Tennant, Performance of a cooled sapphire and beryllium assembly for filtering of thermal neutrons, *Rev. Sci. Instrum.* **59**, 380 (1988).
- [58] M. Mourigal, M. Enderle, A. Klöpperpieper, J.-S. Caux, A. Stunault, and H. M. Rønnow, Fractional spinon excitations in the quantum Heisenberg antiferromagnetic chain, *Nat. Phys.* **9**, 435 (2013).
- [59] L. S. Wu, S. E. Nikitin, Z. Wang, W. Zhu, C. D. Batista, A. M. Tsvelik, A. M. Samarakoon, D. A. Tennant, M. Brando, L. Vasylichko, M. Frontzek, A. T. Savici, G. Sala, G. Ehlers, A. D. Christianson, M. D. Lumsden, and A. Podlesnyak, Tomonaga-Luttinger liquid behavior and spinon confinement in YbAlO_3 , *Nat. Commun.* **10**, 698 (2019).
- [60] G. Xu, Z. Xu, and J. M. Tranquada, Absolute cross-section normalization of magnetic neutron scattering data, *Rev. Sci. Instrum.* **84**, 083906 (2013).
- [61] G. E. Granroth, A. I. Kolesnikov, T. E. Sherline, J. P. Clancy, K. A. Ross, J. P. C. Ruff, B. D. Gaulin, and S. E. Nagler, SEQUOIA: A newly operating chopper spectrometer at the SNS, *J. Phys.: Conf. Ser.* **251**, 012058 (2010).
- [62] T. G. Perring, A. D. Taylor, R. Osborn, D. McK. Paul, A. T. Boothroyd, and G. Aeppli, MAPS: A chopper spectrometer to measure high energy magnetic excitations in single crystals, in *Proceedings of ICANS XII*, RAL Report 94-025 (Rutherford Appleton Laboratory, Didcot, UK, 1994), pp. 1–60.
- [63] H. Ikeda and K. Hirakawa, Neutron diffraction study in one-dimensional antiferromagnet KCuF_3 , *J. Phys. Soc. Jpn.* **35**, 722 (1973).
- [64] S. R. White, Density matrix formulation for quantum renormalization groups, *Phys. Rev. Lett.* **69**, 2863 (1992).
- [65] S. R. White, Density-matrix algorithms for quantum renormalization groups, *Phys. Rev. B* **48**, 10345 (1993).
- [66] A. E. Feiguin and S. R. White, Finite-temperature density matrix renormalization using an enlarged Hilbert space, *Phys. Rev. B* **72**, 220401(R) (2005).
- [67] T. Barthel, U. Schollwöck, and S. R. White, Spectral functions in one-dimensional quantum systems at finite temperature using the density matrix renormalization group, *Phys. Rev. B* **79**, 245101 (2009).
- [68] G. Alvarez, The density matrix renormalization group for strongly correlated electron systems: A generic implementation, *Comput. Phys. Commun.* **180**, 1572 (2009).
- [69] T. D. Kühner and S. R. White, Dynamical correlation functions using the density matrix renormalization group, *Phys. Rev. B* **60**, 335 (1999).
- [70] A. Nocera and G. Alvarez, Spectral functions with the density matrix renormalization group: Krylov-space approach for correction vectors, *Phys. Rev. E* **94**, 053308 (2016).